Coupled plasmon−LO-phonon modes in $Ga_{1-x}Mn_xAs$

W. Limmer,* M. Glunk, S. Mascheck, A. Koeder, D. Klarer, W. Schoch, K. Thonke, R. Sauer, and A. Waag
Abteilung Halbleiterphysik, Universität Ulm, D-89069 Ulm, Germany
(Received 22 July 2002; published 27 November 2002)

The vibrational and electronic properties of $Ga_{1-x}Mn_xAs$ layers with Mn fractions $0 \leqslant x \leqslant 2.8\%$, grown on GaAs(001) substrates by low-temperature molecular-beam epitaxy, are investigated by micro-Raman spectroscopy and far-infrared (FIR) reflectance spectroscopy. The Raman and FIR spectra are strongly affected by the formation of a coupled mode of the longitudinal optical phonon and the hole plasmon. The spectral line shapes are modeled using a dielectric function where intraband and interband transitions of free holes are included. In addition to the coupled mode, the contributions of a surface depletion layer as well as a symmetry forbidden TO phonon have to be taken into account for the Raman spectra. Values for the hole densities are estimated from a full line-shape analysis of the measured spectra. Annealing at temperatures between 250 and 500 °C results in a decrease of the hole density with increasing annealing temperature and total annealing time. Simultaneously, a reduction of the fraction of Mn atoms on Ga lattice sites is deduced from high-resolution x-ray diffraction.

DOI: 10.1103/PhysRevB.66.205209 PACS number(s): 78.30.Fs, 75.50.Pp, 71.45.−d, 61.50.Nw

I. INTRODUCTION

During the past years the idea of utilizing the spin of carriers in novel spintronic devices has led to great efforts in fabricating and investigating appropriate new semiconductor materials. Being compatible with conventional GaAs semiconductor technology, the semimagnetic semiconductor $Ga_{1-x}Mn_xAs$ is one of them.[1,2] Its magnetic properties arise from the $S=5/2$ Mn spin system which undergoes a ferromagnetic phase transition at a maximum Curie temperature of 110 K, as reported so far.[3] The incorporation of Mn atoms on Ga lattice sites, where Mn acts as an acceptor, results in a high hole density, which is assumed to play an important role in the indirect ferromagnetic Mn-Mn-interaction.[4] Measurement of the hole concentration is difficult, since the ordinary Hall effect, normally used to determine carrier densities, is superimposed by a dominating anomalous Hall effect. In the recent past, the properties of $Ga_{1-x}Mn_xAs$ have mainly been studied by magnetotransport, superconducting quantum interference device measurements, and high-resolution x-ray diffraction (HRXRD). Optical investigations on this material system are very limited,[5,6] since the low-temperature growth of $Ga_{1-x}Mn_xAs$ in combination with the metallic doping due to Mn results in a very complex situation. Therefore many basic properties of $Ga_{1-x}Mn_xAs$ are still unknown.

In this work the vibrational and electronic properties of $Ga_{1-x}Mn_xAs$ are studied by both Raman spectroscopy and far-infrared (FIR) reflectance. Model calculations of the spectral line shapes are presented, based on a dielectric function which includes intraband and interband transitions between the valence bands of light and heavy holes.[7] From that, values for the hole densities are estimated.[8] Furthermore, the influence of annealing on the hole density and on the occupation of Ga lattice sites by Mn atoms is studied by Raman spectroscopy and by HRXRD.

II. EXPERIMENTAL DETAILS

The $Ga_{1-x}Mn_xAs$ layers were grown in a RIBER 32 molecular-beam epitaxy (MBE) machine on In-mounted semi-insulating VGF GaAs(001) substrates using solid metal sources as well as an arsenic cracker in the noncracking mode. The III/V beam equivalent pressure (BEP) ratio was 1/10. First, a 100-nm-thick buffer layer was grown at a temperature of $T_g = 585\,°C$, then the growth was interrupted and T_g was lowered to 250 °C, calibrated with the melting points of In and Sn. This extremely low substrate temperature leads to the incorporation of excess As on the order of 1–2%.[9] The properties of low-temperature (LT) grown GaAs have been discussed in detail elsewhere.[10] The fractions of Mn atoms on Ga lattice sites in the 0.6–0.8 μm-thick $Ga_{1-x}Mn_xAs$ layers were determined from HRXRD measurements of the symmetric (004) reflection using a Siemens D5000 diffractometer. The lattice constant of $Ga_{1-x}Mn_xAs$ was calculated, assuming Vegard's law to be valid, with a lattice constant of 0.565 33 nm for GaAs and 0.598 nm for the hypothetical cubic MnAs.[1] All $Ga_{1-x}Mn_xAs$ layers were fully strained as followed from measurements of the asymmetric (115) reflection. More details on the growth of the $Ga_{1-x}Mn_xAs$ samples and results of magnetotransport studies were presented elsewhere.[11]

The micro-Raman measurements were performed at room temperature (RT) using the 514- or 458-nm line of an Ar^+ laser as an excitation source. The laser beam was focused by a microscope lens system yielding a spot diameter of 0.7 μm. The excitation density was kept below 2×10^4 W/cm^2 in order to avoid a heating of the sample and to keep the concentration of optically generated charge carriers negligibly low. The Raman signals were detected in the backscattering configurations $\bar{z}(y',y')z$ and $\bar{x}'(y',y')x'$ using a DILOR XY 800-mm triple-grating spectrometer with a confocal entrance optics and a LN_2-cooled charge-coupled device detector. We denote the [110], [$\bar{1}$10], and [001] directions of the crystal by x', y', and z, respectively. Line scans on cleaved (110) side faces along the [001] growth direction in $\bar{x}'(y',y')x'$ configuration were obtained by slightly shifting the sample position between subsequent measurements. The FIR reflectance spectra were recorded at

 ©2002 The American Physical Society

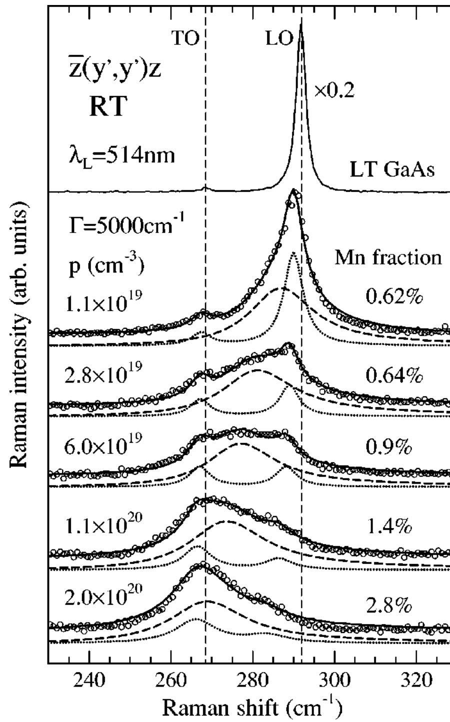

FIG. 1. RT Raman spectra (open circles) recorded in $\bar{z}(y',y')z$ backscattering configuration at the (001) surfaces of $Ga_{1-x}Mn_xAs$ layers with different Mn fractions x. The hole densities p were estimated from a full line-shape analysis (solid lines) including scattering by CPLP modes (dashed lines). Additional contributions (dotted lines) arise from the symmetry forbidden TO phonon and from the LO phonon in the depletion layer.

RT and at normal incidence using a BOMEM DA8 Fourier transform spectrometer equipped with a LHe-cooled bolometer.

III. RESULTS AND DISCUSSION

In Fig. 1 the Raman spectra of five $Ga_{1-x}Mn_xAs$ layers with Mn fractions between 0.62% and 2.8% (open circles) are shown in comparison with the Raman spectrum of a LT-grown GaAs layer. The excitation laser wavelength was 514 nm. In the $\bar{z}(y',y')z$ backscattering configuration scattering by LO phonons is allowed according to the Raman selection rules which are determined by the deformation-potential and the Fröhlich electron-phonon interaction, whereas scattering by transverse optical (TO) phonons is forbidden. With increasing Mn fraction x the LO-phonon line at 292 cm^{-1} broadens and shifts from the LO-phonon position to the TO-phonon position. This behavior is typical for a heavily doped semiconductor with free carriers of very low mobility.[7,12] It arises from the strongly damped longitudinal vibration of the carrier plasma, i.e., the plasmon, which couples with the LO phonon via their macroscopic electric fields to a phononlike coupled plasmon–LO-phonon (CPLP) mode. The plasmon-like part of the CPLP mode is overdamped and cannot be observed. In $Ga_{1-x}Mn_xAs$ the carriers are holes, which originate from the acceptor Mn. In order to study the modification of the electronic and vibrational properties with increasing Mn concentration in more detail, we have performed a line-shape analysis of the Raman spectra. The line shape of the CPLP mode was modeled within the linear-response formalism using a random-phase-approximation dielectric function, which takes into account finite-lifetime effects in a relaxation-time approximation.[13] It includes wave-vector-dependent intraband transitions within the light- and heavy-hole bands as well as interband transitions between them. For reasons of simplicity the valence bands were assumed to be parabolic and isotropic. For the effective light-hole and heavy-hole masses we used the values $m_{lh}=0.08m_0$ and $m_{hh}=0.56m_0$, respectively, where m_0 denotes the free-electron mass. Further parameters, which enter into the model calculations, are the high-frequency dielectric constant $\varepsilon_\infty=10.6$, the Faust-Henry coefficient $C=-0.48$, and the scattering wave vector $\boldsymbol{q}=\boldsymbol{q}_L-\boldsymbol{q}_S=1.04\times10^6$ cm^{-1}, where $\boldsymbol{q}_L$ ($\boldsymbol{q}_S$) denotes the wave vector of the laser (scattered) light. Since these values were not available for $Ga_{1-x}Mn_xAs$, we used those for GaAs.[7] In Fig. 1 the calculated line shapes of the CPLP mode are drawn by dashed lines. Obviously, the measured Raman line shapes cannot be modeled solely by the CPLP band. Two further contributions have to be taken into account, which can be described by Lorentzian line shapes, drawn by dotted lines. The first one is a TO-phonon signal, which is symmetry forbidden in this scattering configuration. It arises from the large numerical aperture of the microscope lens system and, especially for higher Mn fractions, from disorder-induced scattering. The second one is the LO-phonon signal from a depletion layer near the sample surface. In the depletion layer, no free holes are present, and therefore no coupling between LO phonons and hole plasmons occurs. Considering a superposition of the three contributions, drawn by solid lines in Fig. 1, an excellent agreement between the measured Raman spectra and the calculated line shapes can be achieved.

The frequencies and linewidths of the TO- and LO-phonon lines, which enter as crucial parameters into the model calculations of the CPLP line shape, strongly depend on the Mn fraction x. They have to be known for a reliable analysis of the spectra. Therefore we have determined their x dependence from spatially resolved micro-Raman measurements on cleaved (110) side faces and from Raman measurements using the 458-nm line of the Ar^+ laser as an excitation source. Figure 2 exhibits a Raman line scan on the cleaved (110) surface of the sample with $x=2.8\%$ along the [001] direction. In the $\bar{x}'(y',y')x'$ backscattering configuration scattering by TO phonons is allowed and scattering by LO phonons is forbidden according to the Raman selection rules. The sample was laterally shifted by 0.25 μm between subsequent measurements. In the $Ga_{1-x}Mn_xAs$ layer the full width at half maximum (FWHM) of the TO-phonon line is increased and its frequency is shifted to smaller wave numbers compared to the TO-phonon line in the GaAs substrate. The values for the frequency shift and for the FWHM were determined from the spectra recorded at the interface between air and $Ga_{1-x}Mn_xAs$ layer, where no contribution of the phonon signal from the GaAs substrate is present. Similar line scans were performed for all samples under investigation. In addition to these results, further values for the

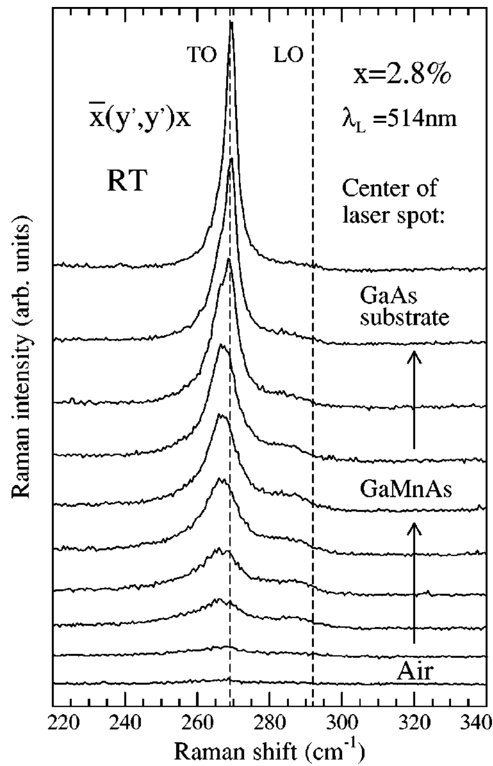

FIG. 2. RT micro-Raman line scan on the cleaved (110) surface of the sample with 2.8% Mn concentration in $\bar{x}'(y',y')x'$ backscattering configuration along the [001] growth direction. The sample position between subsequent measurements was shifted by 0.25 μm.

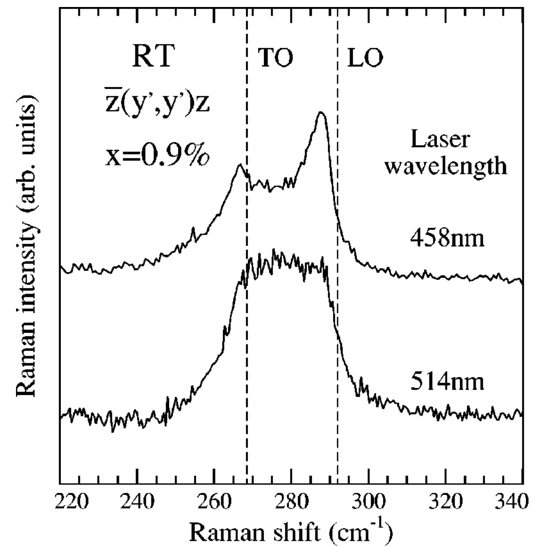

FIG. 3. Comparison between two Raman spectra recorded from the same sample ($x=0.9\%$) using different laser wavelengths of 458 and 514 nm.

frequency shift and for the FWHM of both TO and LO phonons were derived from Raman spectra excited by the 458-nm line of the Ar^+ laser. For this wavelength the light-penetration depth is only $1/\alpha_{458} \approx 50$ nm in comparison with $1/\alpha_{514} \approx 100$ nm for the 514-nm laser line, where α denotes the absorption coefficient. Therefore, the relative strength of the signal arising from the depletion layer is larger, and the LO-phonon mode can be well separated from the CPLP mode. This is demonstrated in Fig. 3 for the sample with $x=0.9\%$: Only for the excitation with 458 nm the TO- and LO-phonon lines are clearly discernible. Both the TO- and the LO-phonon lines are shifted to lower frequencies relative to those of LT GaAs (dashed lines). In Fig. 4 the values for the frequency shift and the FWHM, derived in the two ways described above, are depicted in dependence on x by filled and open stars for the TO phonon, and by filled and open squares for the LO phonon, respectively. We ascribe the observed x dependences mainly to alloying effects, which result, e.g., in a reduction of the bonding forces and in a lifting of the translational symmetry of the crystal lattice. As a consequence, the scattering wave vector $\boldsymbol{q}$ is not strictly conserved in the scattering process, leading to a redshift and a broadening of the TO- and LO-phonon lines. The compressive strain in the $Ga_{1-x}Mn_xAs$ layers should lead to a blueshift of the phonon frequencies, but is obviously overcompensated by the alloying effects.

For the line-shape analysis of the Raman spectra in Fig. 1, the plasmon damping Γ and the hole density p were treated as fit parameters. We found that satisfactory fits were not only obtained for one pair of p and Γ, but for a continuum of pairs. Therefore the line-shape calculations were performed as follows: For a given value of the plasmon damping Γ the hole density p was varied until the best possible agreement between the calculated and the measured spectrum was achieved. In this way, for each sample a relation $p(\Gamma)$ for the optimal fit curve was derived. In Fig. 5 the x-dependent relations $p(\Gamma)$ are depicted, which turn out to be nearly linear. This linearity can be made plausible even in a simplified Drude model, where interband transitions are neglected and only one type of carrier is considered. Assuming $\boldsymbol{q}=0$ as well as $\Gamma \gg \omega_{LO,TO}$, the plasmon contribution $\varepsilon_{plasmon}$ to the total dielectric function can be written as[7]

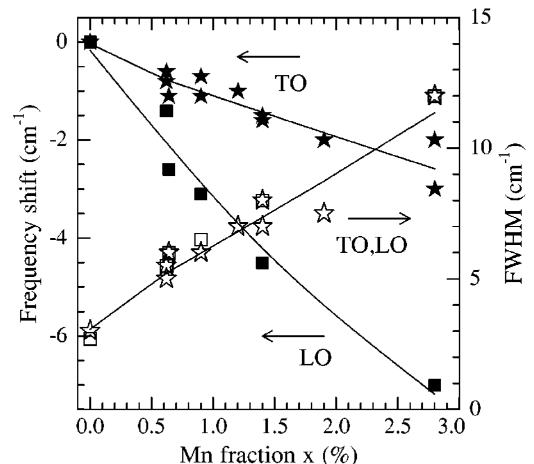

FIG. 4. Frequency shifts of the TO phonon (filled stars) and LO phonon (filled squares) Raman lines, and broadening (FWHM) of the TO phonon (open stars) and LO phonon (open squares) Raman lines as a function of Mn fraction.

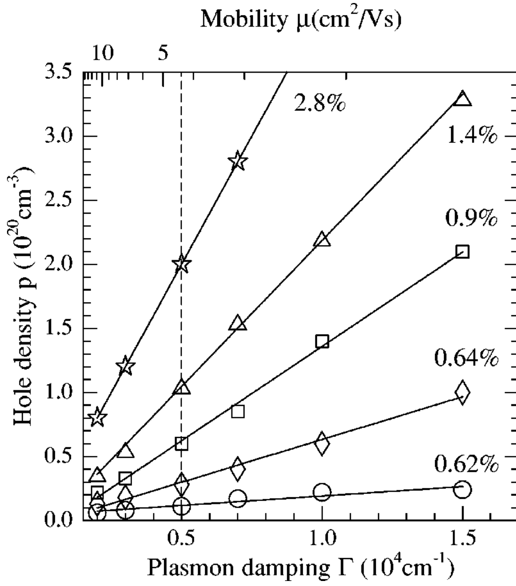

FIG. 5. Hole densities p derived from a full line-shape analysis of the Raman spectra in dependence on the plasmon damping Γ used in the model calculations.

$$\varepsilon_{plasmon}(\omega) = -\frac{\varepsilon_\infty \omega_p^{*2}}{\omega(\omega + i\Gamma)} \approx i\frac{e^2}{\omega\varepsilon_0 m_h^*}\frac{p}{\Gamma}, \qquad (1)$$

where $\omega_p^{*2} = e^2 p/\varepsilon_0\varepsilon_\infty m_h^*$ denotes an effective plasmon frequency, e the elemental charge, and

$$m_h^* = \frac{m_{lh}^{3/2} + m_{hh}^{3/2}}{m_{lh}^{1/2} + m_{hh}^{1/2}} \qquad (2)$$

an effective hole mass. From the right-hand side in Eq. (1) it follows that the same $\varepsilon_{plasmon}(\omega)$, and thus the same line shape is obtained by keeping the ratio p/Γ fixed. However, in the more sophisticated model used for our calculations the degree of coincidence between the calculated and the measured curves is not always the same over the whole range of Γ depicted in Fig. 5. The best results are obtained for $\Gamma \geqslant 5000\ \mathrm{cm}^{-1}$. This corresponds to a hole mobility of $\mu_h \leqslant 4\ \mathrm{cm}^2/\mathrm{V\,s}$, which is calculated from the relation

$$\mu_h = \frac{e}{2\pi c m_h^*}\frac{1}{\Gamma}, \qquad (3)$$

where c denotes the speed of light in vacuum. All line shapes in Fig. 1 were calculated with $\Gamma = 5000\ \mathrm{cm}^{-1}$ for both light holes and heavy holes. The corresponding hole densities range from $p = 1.1\times10^{19}\ \mathrm{cm}^{-3}$ for $x = 0.62\%$ up to $p = 2\times10^{20}\ \mathrm{cm}^{-3}$ for $x = 2.8\%$.

It should be emphasized that a line-shape analysis of the CPLP mode would strongly underestimate the hole concentration at high Mn fractions, if the small LO-phonon linewidth from the GaAs substrate was used in the calculations instead of that from the $Ga_{1-x}Mn_xAs$ layer. Furthermore, using only a simple Drude model for the dielectric function, which cannot account for interband transitions, significantly different line shapes would be obtained for the CPLP modes.

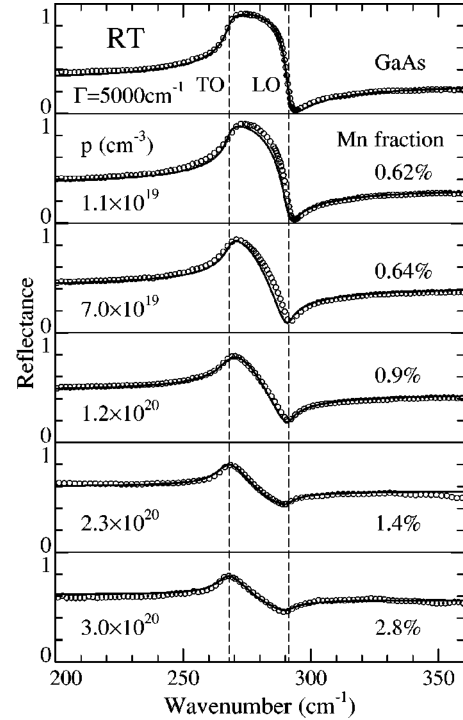

FIG. 6. RT FIR reflectance spectra recorded at normal incidence. The hole densities p were estimated from a full line-shape analysis (solid lines) considering multiple reflections within the $Ga_{1-x}Mn_xAs$ layer.

In general, the line-shape analysis of Raman spectra has two merits: First, if the hole mobility is known from other (e.g., electrical) measurements, the hole density can be determined with high accuracy, and vice versa. Second, micro-Raman spectroscopy can be performed with a high spatial resolution, and hence information on the spatial variation of the carrier concentration can be derived. Moreover, in $Ga_{1-x}Mn_xAs$ the determination of hole densities by Hall measurements is extremely problematic, since the ordinary Hall effect is superimposed by a dominating anomalous Hall effect.[1]

Figure 6 exhibits RT FIR reflectance spectra (open circles) recorded at normal incidence from the same samples as in Fig. 1. Similar to the Raman spectra, a clear dependence of the reflectance line shape on the Mn fraction x is observed: With increasing x the Reststrahlen band between the frequencies of the TO phonon and the LO phonon flattens and the total amount of reflectance increases. Again, the change in the line-shape mainly arises from the plasmon contribution to the dielectric function in the $Ga_{1-x}Mn_xAs$ layer. We have performed a full line shape analysis (solid lines) of the FIR reflectance spectra and found that the measured curves can only be modeled if the finite thickness of the $Ga_{1-x}Mn_xAs$ layer, the interface between the layer and the GaAs substrate, and multiple reflections within the layer are taken into account. Therefore the calculations were based on a sample system which consists of a thin $Ga_{1-x}Mn_xAs$ layer on top of a semi-infinite GaAs substrate, surrounded by air. No significant influence by a thin depletion layer on the spectra could be found. The formula used for the calculation

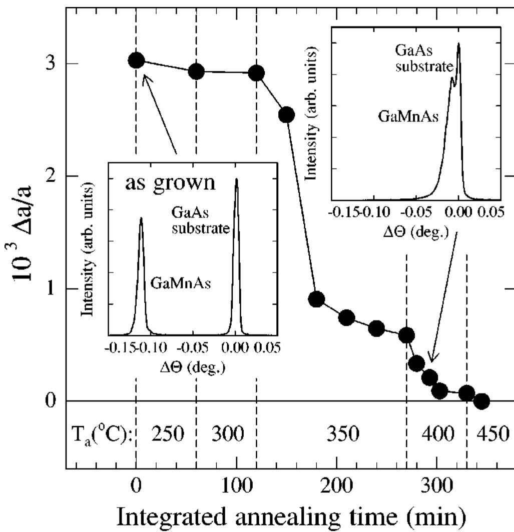

FIG. 7. Relative change of the lattice constant a in dependence on the annealing temperature T_a and on the integrated annealing time of the sample with (as-grown) 2.8% Mn. The insets show measured HRXRD spectra with contributions from the GaMnAs layer and the GaAs substrate.

of the complex-amplitude reflection coefficient were taken from Ref. 14, where an extensive theoretical description of FIR reflection at multilayer structures is given. The dielectric function in the $Ga_{1-x}Mn_xAs$ layer was calculated within the same model as in the case of the Raman analysis, i.e., both intraband and interband transitions between parabolic heavy-hole and light-hole valence bands were taken into account. According to the large wavelength of the FIR light the scattering wave vector can be approximated by $\boldsymbol{q}\approx 0$. Since FIR reflection and Raman scattering by CPLP modes are based on the same dielectric function, the same ambiguity holds for the values of p and Γ, derived from a line-shape analysis of the measured spectra. Using again the value of $\Gamma = 5000\ \mathrm{cm}^{-1}$ for the plasmon damping, very good fits to the measured FIR reflectance curves were obtained. The hole densities p derived from FIR reflectance are up to a factor of 2.5 higher than those obtained from the Raman measurements. They range from $p=1.1\times 10^{19}\ \mathrm{cm}^{-3}$ for $x=0.62\%$ up to $p=3\times 10^{20}\ \mathrm{cm}^{-3}$ for $x=2.8\%$. Furthermore, somewhat smaller values for the phonon frequency shift and the FWHM had to be used. These differences may be the consequence of inhomogeneities in the $Ga_{1-x}Mn_xAs$ layers along the growth direction in combination with the different probing depths of Raman and FIR reflectance spectroscopy.

In order to study the influence of annealing on the CPLP mode and on the occupation of Ga lattice sites by Mn atoms, the sample with (as grown) $x=2.8\%$ was annealed several times in air at various successively increased temperatures between 250 and 500 °C. After each annealing step the sample was characterized at RT by HRXRD and by Raman spectroscopy. The results are shown in Figs. 7 and 8, respectively. In Fig. 7 the relative change $\Delta a/a$ of the lattice constant a is shown as a function of the integrated annealing time. Annealing for 60 min at 250 °C and additional 60 min at 300 °C does not significantly change the hole density and the Mn fraction. This can be concluded from the almost identical line shapes of the corresponding Raman spectra in Fig. 8 and from the nearly constant value of $\Delta a/a$ in Fig. 7. At 350 °C the CPLP mode starts to shift from the TO-phonon to the LO-phonon frequency indicating a reduction of the hole concentration with increasing annealing temperature and total annealing time. Simultaneously, a decrease of the number of Mn atoms on Ga lattice sites is observed in HRXRD where $\Delta a/a$ tends to zero. After annealing at 450 °C the Mn fraction is lower than 0.1%, as deduced from $\Delta a/a$. No sig-

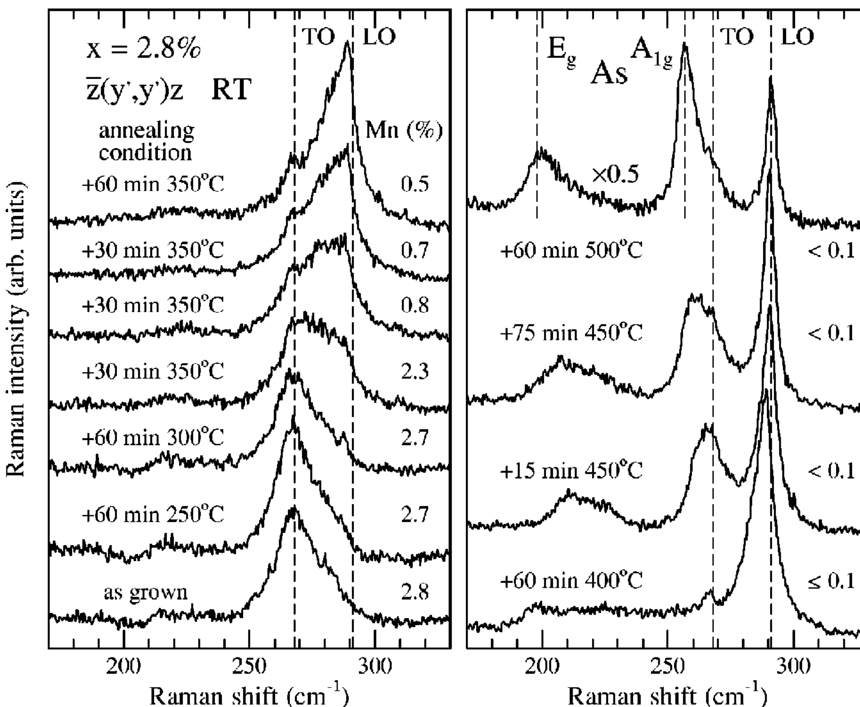

FIG. 8. Raman spectra recorded from the sample with 2.8% Mn after annealing at various successively increased temperatures. The fraction of Mn atoms on Ga lattice sites was deduced from HRXRD.

nificant influence of free carriers on the Raman line shape is further observed, and the LO-phonon mode appears as a sharp line. Furthermore, the Raman lines of elemental As arise, which are due to the precipitation of excess As on the sample surface, as confirmed by atomic force microscopy. The observed decrease of $\Delta a/a$ due to annealing is in agreement with the results reported in Ref. 2, where the extraction of the Mn atoms from the $Ga_{1-x}Mn_xAs$ lattice is attributed to the formation of MnAs donor complexes.[15] The reduction of the Mn acceptor concentration in combination with compensation by MnAs complexes leads to the decrease of the hole density, clearly monitored by the Raman spectra.

IV. CONCLUSIONS

We have investigated the vibrational and electronic properties of $Ga_{1-x}Mn_xAs$ layers with $0 \leqslant x \leqslant 2.8\%$ by Raman and FIR reflectance spectroscopy. The spectra can be well modeled taking into account the phononlike coupled mode of the hole plasmon and the LO phonon. The dielectric function was calculated including intraband and interband transitions between the light-hole and heavy-hole valence bands. For the Raman line shapes a surface depletion layer as well as a symmetry forbidden TO phonon had to be considered. The x dependences of the TO- and LO-phonon frequencies and FWHM's, which enter as crucial parameters into the calculations, were determined experimentally. From a full line-shape analysis of the Raman and FIR reflectance spectra, the possible pairs (p,Γ) of hole density p and plasmon damping Γ, giving a good coincidence between theoretical and experimental results, were derived for each sample. For a plasmon damping of $\Gamma = 5000\ \mathrm{cm}^{-1}$ estimated values for p range between $1.1\times 10^{19}\ \mathrm{cm}^{-3}$ for $x = 0.62\%$ and $3.0\times 10^{19}\ \mathrm{cm}^{-3}$ for $x = 2.8\%$. Subsequent annealing at temperatures between 250 and 500 °C results in a reduction of the number of Mn atoms on Ga sites and in a decrease of the hole density, as deduced from HRXRD and Raman measurements.

*Electronic address: wolfgang.limmer@physik.uni-ulm.de; URL: http://hlhp1.physik.uni-ulm.de

[1] H. Ohno, Science **281**, 951 (1998).

[2] A. Van Esch, L. Van Bockstal, J. De Boeck, G. Verbanck, A.S. van Steenbergen, P.J. Wellmann, B. Grietens, R. Bogaerts, F. Herlach, and G. Borghs, Phys. Rev. B **56**, 13 103 (1997).

[3] F. Matsukura, H. Ohno, A. Shen, and Y. Sugawara, Phys. Rev. B **57**, R2037 (1998).

[4] T. Dietl, H. Ohno, and F. Matsukura, Phys. Rev. B **63**, 195205 (2001).

[5] Y. Nagai, T. Kunimoto, K. Nagasaka, H. Nojiri, M. Motokawa, F. Matsukura, T. Dietl, and H. Ohno, Jpn. J. Appl. Phys., Part 1 **40**, 6231 (2001).

[6] W. Heimbrodt, T. Hartmann, P.J. Klar, M. Lampalzer, W. Stolz, K. Volz, A. Schaper, W. Treutmann, H.-A. Krug von Nidda, A. Loidl, T. Ruf, and V.F. Sapega, Physica E (Amsterdam) **10**, 175 (2001).

[7] G. Irmer, M. Wenzel, and J. Monecke, Phys. Rev. B **56**, 9524 (1997), and references therein.

[8] W. Limmer, M. Glunk, W. Schoch, A. Koeder, R. Kling, R. Sauer, and A. Waag, Physica E (Amsterdam) **13**, 589 (2002).

[9] S. O'Hagan and M. Missous, J. Appl. Phys. **75**, 7835 (1994).

[10] M.R. Melloch, J.M. Woodall, E.S. Harmon, N. Otsuka, F.H. Pollak, D.D. Nolte, R.M. Feenstra, and M.A. Lutz, Annu. Rev. Mater. Sci. **25**, 547 (1995).

[11] A. Koeder, W. Schoch, S. Frank, R. Kling, M. Oettinger, V. Avrutin, W. Limmer, R. Sauer, and A. Waag, in *Proceedings of the 10th International Symposium "Nanostructures: Physics and Technology," St. Petersburg, 2002* (in press).

[12] G. Abstreiter, M. Cardona, and A. Pinczuk, in *Light Scattering in Solids IV*, edited by M. Cardona and G. Güntherodth (Springer, Berlin, 1984), p. 5.

[13] G. Irmer, J. Monecke, and M. Wenzel, J. Phys.: Condens. Matter **9**, 5371 (1997).

[14] B. Harbecke, B. Heinz, V. Offermann, and W. Theiß, in *Optical Characterization of Epitaxial Semiconductor Layers*, edited by G. Bauer and W. Richter (Springer, Berlin, 1996), p. 203.

[15] A. Krol, Y.L. Soo, S. Huang, Z.H. Ming, Y.H. Kao, H. Munekata, and L.L. Chang, Phys. Rev. B **47**, 7187 (1993).